Textures and Microstructures, 2002, Vol. 35(2), pp. 55–70

Taylor & Francis
Taylor & Francis Group

RECRYSTALLIZATION IN A HOT DEFORMED Al-Mg-Si ALLOY: THE EFFECT OF FINE PRECIPITATES

S. DE LA CHAPELLE[a,*] and P. DUVAL[b,†]

[a]*Centre SMS, Ecole des Mines de Saint Etienne, 158 Cours Fauriel, 42023 Saint Etienne Cedex 2, France;* [b]*Laboratoire de Glaciologie et Géophysique de l'Environnement, CNRS, B.P. 96, 38402 St. Martin d'Hères Cedex, France*

(Received 15 November 2001)

The recrystallization of an Al-Mg-Si alloy deformed by plane strain compression at 400°C and 1 s^{-1} has been studied. Fine particles are found to have a significant influence on the development of recrystallization textures. Annealing at 400°C, in the presence of Al-Fe-Si particles located on boundaries, results in a weak recrystallization texture. There is a clear indication that grain nucleation is associated with abnormal subgrain growth. The occurrence of this recovery process is analyzed by taking into account the particle pinning pressure and the orientation dependence of boundary energy and mobility. The cube recrystallization texture observed after annealing at 510°C is discussed in terms of the stability of Mg_2Si and Al-Fe-Si precipitates.

Keywords: Electron diffraction; Aluminum alloys; Texture; Subgrain growth; Recovery; Recrystallization

1. INTRODUCTION

The control of grain size and texture during the thermomechanical processing of aluminum alloys is of the highest importance for industrial applications. The recrystallization behavior of alloys containing dispersions of large and small particles has been the subject

*Corresponding author. E-mail: schapelle@scconsultants.com. Present address: Science & Computers Consultants, Parc Giron, 8 rue de la Richelandière 42100 St. Etienne, France

ISSN 0730-3300 print/ISSN 1029-4961 online
DOI: 10.1080/0730330021000000209

of numerous investigations (Humphreys and Haterly, 1995). The large particles can promote recrystallization through particle stimulated nucleation (Humphreys, 1977). This mechanism generally leads to a wide range of nucleus orientations and consequently to a weak recrystallization texture (Chan and Humphreys, 1984; Humphreys and Haterly, 1995). The small particles can inhibit recrystallization by pinning the migrating subgrain and grain boundaries (Smith, 1948; Nes, 1976). Such dispersoids induce a Zener pinning pressure ($\mathbf{P}_z$) and, as a consequence, the critical nucleus must be sufficiently large to overcome the conditions given by the Gibbs–Thompson relationship (Nes, 1976). Due to the size advantage of cube subgrains, a strengthening of the cube, (100) ⟨001⟩, texture can be observed (Ridha and Hutchinson, 1982; Vatne *et al*., 1996; Benum and Nes, 1997). The variation of the Zener pressure with boundary orientation can also induce sharpness in the cube recrystallization texture (Humphreys and Ardakani, 1996; Daaland and Nes, 1996; Higginson *et al*., 1997). The preferential growth of cube grains during recrystallization could be due to low Zener pinning on special grain boundaries associated with the orientation relationship between the cube orientation and components of the rolling texture close to the S (123) $\langle 63\bar{4} \rangle$ orientation (Higginson *et al*., 1997).

As stated by Humphreys (1997a), recovery by subgrain growth can also be inhibited by fine particles. The limiting subgrain size obtained by normal growth can be lower than that needed to initiate nucleation. Recrystallization can however occur after recovery by abnormal subgrain growth. Such a mechanism was analyzed by Humphreys (1997a). The theory is based on the stability of cellular structures as developed for abnormal grain growth (Hillert, 1965; Rollett *et al*., 1989). The orientation dependence of boundary energy and mobility is taken into account. It appears that a subgrain will grow abnormally if its size is sufficiently large and if its misorientation is higher than the mean misorientation of the subgrain assembly. A subgrain can be a successful nucleus if its size is large enough to overcome the nucleation conditions. Under these conditions, the size advantage of cube oriented subgrains (Vatne *et al*., 1996; Benum and Nes, 1997; Samadjar and Doherty, 1998) cannot be a prerequisite since both the size and misorientation of subgrains control discontinuous subgrain growth (Humphreys, 1997a).

The present work was carried out in order to assess the role of fine particles in recovery and recrystallization, using an Al-Mg-Si alloy. Various precipitation states were introduced by different annealing treatments. Special emphasis is placed on the development of recrystallization textures. The effect of dispersoids on the recrystallization behavior is analyzed according to the approach of Humphreys (1997a,b) based on the stability of cellular microstructures.

2. EXPERIMENTAL

2.1. Material

All experiments were carried out on a AA6060 aluminum alloy with the composition given in Table I. The small amount of manganese does not limit the grain boundary mobility. Depending on the heat treatment, this alloy can contain hardening precipitates. The starting material was in a recrystallized condition containing 30% cube (Fig. 1) and a quasi-equiaxed grain structure with a mean size of 60 μm. By cutting samples along specific directions, specimens with about 30% Goss (110) ⟨001⟩ orientation were obtained. The Goss orientation was chosen because grains generally exhibit homogeneous deformation (Akef, 1993; Ferry and Humphreys, 1996).

2.2. Heat Treatment and Precipitation

Before deformation, samples were solubilized during 20 min at 500°C in a salt bath and heat treated for 1 or 24 h at 400°C in an air furnace and then water quenched. Samples are therefore respectively referenced as *Goss1h* and *Goss24h*. The two heat treatments were chosen in order to obtain various precipitation microstructures. Indeed, during annealing at 400°C, Mg_2Si particles form and progressively

TABLE I Chemical composition of the 6060 alloy

	Mg	*Si*	*Fe*	*Cu*	*Mn*	*Cr*	*Zn*	*Ti*	*Ni*
Weight%	0.44	0.42	0.21	0.01	0.007	0.004	0.01	0.009	0.002

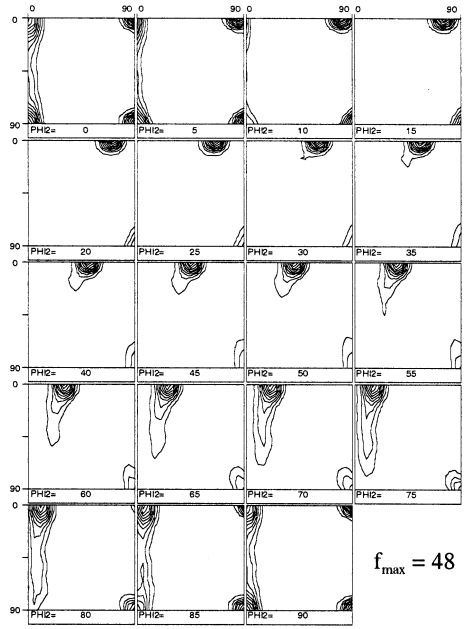

FIGURE 1 ODF of the Al-Mg-Si alloy as received.

coarsen with time (Zajac *et al*., 1996), whereas the Al-Fe-Si particles are relatively stable at this temperature. Due to the low content of Mg and Si in this alloy and the low contrast between the aluminum matrix and the Mg_2Si precipitates, it was not possible to observe these precipitates by Transmission Electron Microscopy (TEM). The Al-Fe-Si precipitates, observed in deformed samples, were found located on boundaries (Figs. 2a and b). They are cylindrical in shape and their size depends on the heat treatment duration. The diameter of such precipitates is 30 nm for the *Goss1h* sample and 50 nm for the *Goss24h* sample. The lengths are respectively 60 and 100 nm.

2.3. Thermomechanical Process

Samples were deformed by high temperature plane strain compression in a channel die equipped with a retractable side wall which enables the

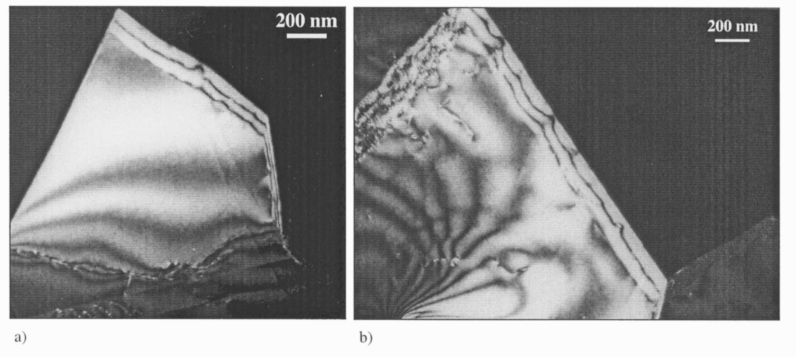

FIGURE 2 TEM micrographs of the Goss samples after hot deformation in plane strain compression showing Al-Fe-Si precipitates located on boundaries. 2a: *Goss1h*; 2b: *Goss24h*.

sample to be extracted from the die and then water quenched within 2–3 s of the deformation (Maurice and Driver, 1993). The channel die equipment was used in a computer controlled Instron screwdriven machine to ensure a constant strain rate. The samples were wrapped in Teflon films and the tool surfaces greased with a graphite spray mixture to reduce friction effects. They were deformed to a Von Mises strain $\varepsilon = 1.5$, at a strain rate $\dot{\varepsilon} = 1\,\mathrm{s}^{-1}$ and a temperature $T = 400^{\circ}\mathrm{C}$. The samples were recrystallized in a salt bath during 10 min at 400°C and 10 s at 510°C.

2.4. Microstructural Characterization

Bulk textures and microstructures were analyzed by using X-ray diffraction and Electron Back Scattered Diffraction (EBSD). An accuracy of $\sim 1^{\circ}$ in the orientation determination and $\sim 0.5\,\mu\mathrm{m}$ in the size of subgrains was obtained with the EBSD technique. Orientation Distribution Functions (ODFs) were produced by following the Bunge's convention (1993). The orientations were defined as those within 15° of the ideal orientations. For transmission electron microscopy, thin foils, prepared by electropolishing 3 mm discs cut from sections parallel to the normal–compression plane of the specimens were examined under a 200 kV electron microscope.

3. RESULTS

3.1. Textures and Microstructure After Deformation

Figure 3 shows the volume fraction of the main orientation components before and after deformation for both Goss samples. As expected (Panchanadeeswaran and Field, 1995), the Goss texture component is relatively stable during plane strain compression and rotation of the lattice towards the β fiber is observed. The cube component is keeping a volume fraction lower than 1% for the two Goss samples.

Table II gives the mean value of the subgrain size $\bar{\delta}$ and subboundary misorientation $\bar{\theta}$ determined by EBSD for the two Goss samples. The subgrain size was determined by calculating the mean distance between low angle boundaries using the mean linear intercept method with scans along the normal direction on a longitudinal section with a step of 0.5 μm. Due to the limitation of the EBSD technique, boundaries of misorientation lower than 1° were excluded from the analysis. For both Goss samples, values of $\bar{\delta}$ and $\bar{\theta}$ are similar. The duration of the heat treatment before deformation therefore has a slight influence on the size and misorientation of subgrains.

The energy stored in the deformation microstructure can be estimated from measurements of subgrain sizes and misorientations.

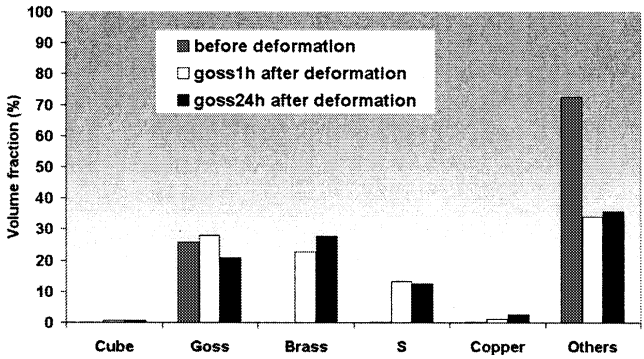

FIGURE 3 Volume fraction of the main orientation components of Goss samples: **grey**: before deformation; **white**: *Goss1h* after deformation; **black**: *Goss24h* after deformation.

TABLE II Subgrain size, misorientations and stored energy for the two Goss samples

	Goss 1 h	*Goss* 24 h
Subgrain size, $\bar{\delta}\,\mu m$	4.9	4.5
Sub-boundary misorientation, $\bar{\theta}$	5.2°	5.6°
Stored energy in sub-boundaries, $E_s(kJ/m^3)$	87	99

By assuming that the density of free dislocations is negligible, the stored energy, E_s is given by:

$$E_s = \frac{\alpha \bar{\gamma}_{sb}}{\bar{\delta}} \tag{1}$$

where α is a geometric constant taken equal to 2 (Huang and Humphreys, 1999) and $\bar{\gamma}_{sb}$ the mean subgrain boundary energy, which is given by the standard Read–Schockley relation (Read, 1953):

$$\bar{\gamma}_{sb} = \gamma_m \frac{\bar{\theta}}{\theta_m}\left(1 - \ln\frac{\bar{\theta}}{\theta_m}\right) \tag{2}$$

γ_m and θ_m represent the boundary energy and misorientation when the boundary becomes high angle (taken to be 15°). In calculations, γ_m is taken as $0.3\,J/m^2$ (Murr, 1975). Values of the stored energy in sub-boundaries deduced from Eq. (1) with measurements of $\bar{\delta}$ and $\bar{\theta}$ are given in Table II. It is important to mention that these values are lower bounds since the energy of free dislocations is not taken into account. On the other hand, due to the limitation of the EBSD technique, values of $\bar{\delta}$ given in Table II are upper bounds. The stored energy in the two Goss samples should be therefore higher than that given in Table II (De La Chapelle, 2000).

3.2. Textures and Microstructures

3.2.1. Recrystallization at 400°C

Figures 4 and 5 show the pole figures, obtained by EBSD for the two Goss samples after recrystallization at 400°C. For the *Goss1h* sample, only ~50 grains were analyzed, but a large part of the specimen was studied. For the *Goss24h* sample, ~150 grains were measured.

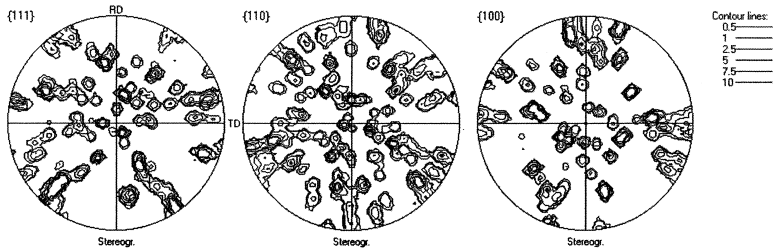

FIGURE 4 Pole figures of the recrystallized *Goss1h* sample at 400°C.

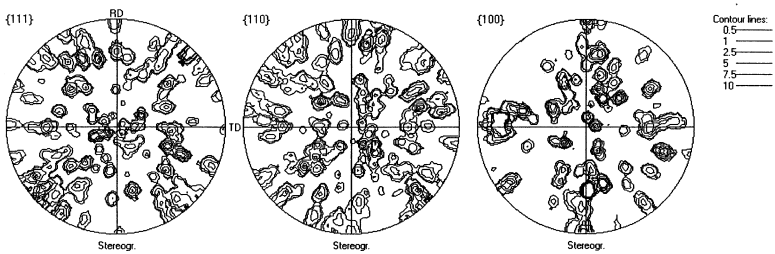

FIGURE 5 Pole figures of the recrystallized *Goss24h* sample at 400°C.

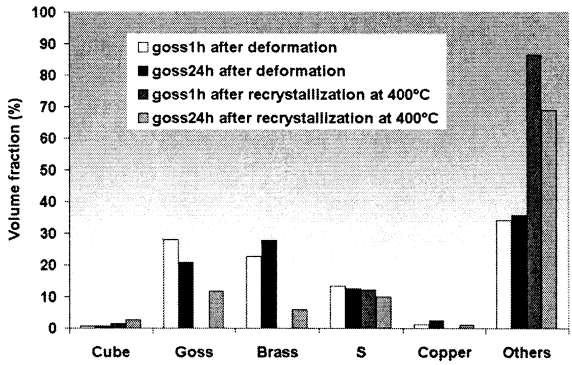

FIGURE 6 Volume fraction of the main orientation components of the two Goss samples after deformation and after recrystallization at 400°C.

A random texture was obtained for both samples. The volume fraction of the cube component is less than 4% for the two Goss samples (Fig. 6). A similar result was found on the same material with 30% cube before deformation (De La Chapelle, 2000). The microstructure

for the two Goss samples after recrystallization is given in Fig. 7. The grain size along ND is about 400 μm for the *Goss1h* sample and only 150 μm for the *Goss24h* sample. Therefore, grain size appears to be depending on the duration of the heat treatment before deformation. This result can be explained by the coarsening of Mg_2Si particles during the heat treatment, whereas the Al-Fe-Si particles are relatively stable (Figs. 2a and b). A decrease of the Zener pressure during the annealing at 400°C would permit a higher number of recrystallization nuclei for *Goss24h*.

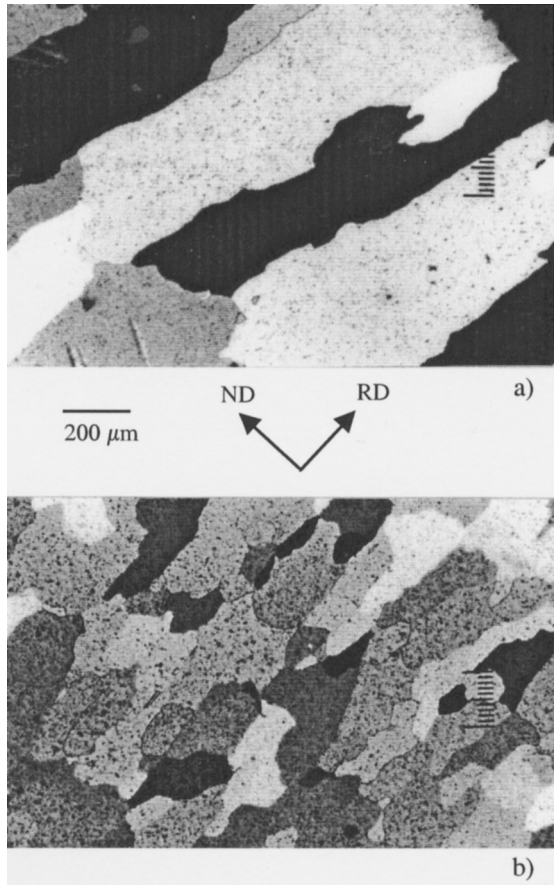

FIGURE 7 Optical micrographs of the deformed Goss samples after annealing at 400°C during 10′; (a) *Goss 1h;* (b) *Goss 24h.*

3.2.2. Recrystallization at 510°C

The volume fraction of the main orientation components in the *Goss1h* sample after recrystallization at 510°C is shown in Fig. 8. Texture appears to be dominated by the cube component in spite of its very low volume fraction before and after deformation. A similar result was obtained with samples exhibiting before deformation about 30% of the copper (112) $\langle 11\bar{1}\rangle$ orientation and less than 1% of cube (De La Chapelle, 2001). At this annealing temperature, Mg_2Si should be dissolved in the first part of the annealing time (Zajac *et al.*, 1996) and Al-Fe-Si precipitates become rapidly coarser by coalescence (De La Chapelle, 2000). Considering the very low volume fraction of the cube component before deformation (< 1%), the nucleation of cube grains from cube bands cannot be invoked. From De La Chapelle, (2000), the nucleation of cube grains would arise from cube subgrains in non-cube grains exhibiting a wide spread of orientations. As suggested by Beaudoing *et al.* (1996), the formation of cube nuclei could be associated with inhomogeneous deformation induced by interactions between neighboring grains. The generation of new cube grains from cube bands does not therefore appear to be the only cause of cube recrystallization textures (Kamijo *et al.*, 1993; Beaudoing *et al.*, 1996).

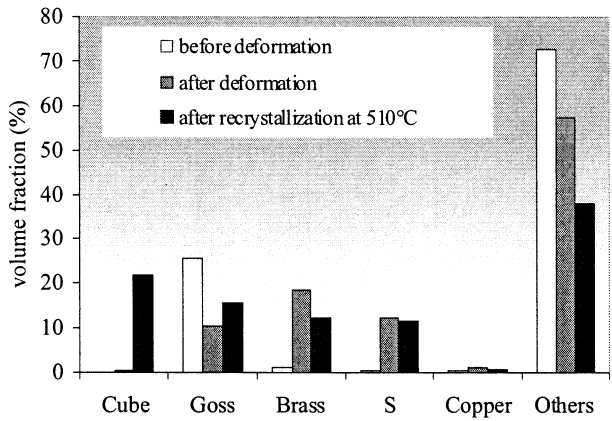

FIGURE 8 Volume fraction of the main orientation components of the *Goss1h*: **white**: before deformation; **grey**: after deformation; **black**: after recrystallization at 510°C during 10″.

4. RECRYSTALLIZATION AT 400°C; EFFECT OF FINE PRECIPITATES

4.1. Zener Pressure

The Zener pressure, $\mathbf{P}_z$, is calculated taking into account the Al-Fe-Si dispersoids. From Smith (1948), the drag force, F_z, exerted by a small precipitate on a sub-boundary is given by:

$$F_z \approx \pi r' \gamma_{\mathrm{sb}} \tag{3}$$

where r' is the equivalent radius determined assuming spherical particles. From TEM measurements, the value of r' is respectively equal to 22 nm for the *Goss1h* sample and 36 nm for the *Goss24h* sample. With particles located only on boundaries, the Zener pressure is equal to:

$$P_z = N_s F_z = \frac{\pi r' \gamma_{\mathrm{sb}}}{d'^2} \tag{4}$$

where $N_s = 1/d'^2$ represents the number of precipitates per unit area of sub-boundary (d' is the mean distance between particles after deformation). As expected, the Zener pressure increases with the misorientation of sub-boundaries and the radius of precipitates.

From Eq. (4), a mean Zener pressure on sub-boundaries, due to Al-Fe-Si precipitates, can be calculated by considering the mean subgrain boundary energy $\bar{\gamma}_{\mathrm{sb}}$. This specific energy determined from the Read–Schockley equation with values of the mean misorientation given in Table II is equal to $0.21\,\mathrm{J/m^2}$ for the *Goss1h* sample and $0.22\,\mathrm{J/m^2}$ for the *Goss24h* sample. The Zener pressure is therefore equal to ~ 20 kPa for *Goss1h* and ~ 30 kPa for *Goss24h*. Note that these values represent lower bounds since the Mg_2Si particles were not taken into account.

4.2. Nucleation By Abnormal Subgrain Growth

A subgrain can be a successful nucleus if its size, δ, is sufficiently large to overcome the Gibbs–Thompson relationship given by:

$$\delta_c = \frac{4\gamma_{\mathrm{gb}}}{E_s - P_z} \tag{5}$$

where E_s is the stored energy and $\gamma_{gb} = 0.3\,J/m^2$ (Huang and Humphreys, 1999). P_z is calculated from Eq. (4) with the specific energy of grain boundaries γ_{gb}.

From values of the stored energy calculated above (Table II), the critical nucleus size, determined from Eq. (5), is about 18 μm for *Goss1h* and about 19 μm for *Goss24h*. With a mean size of subgrains between 4.5–4.9 μm for the two samples and by assuming a log-normal distribution of the subgrain size, the nucleation conditions are not fulfilled for the two Goss samples before annealing. As stated above, the values of the stored energy given in Table II are lower bounds, but higher Zener pressures are expected with the presence of Mg_2Si particles. In spite of these uncertainties, recrystallization in these samples therefore should imply subgrain growth in the early stage of annealing.

The rate of normal subgrain growth in the presence of particles is given by:

$$\frac{d\bar{R}}{dt} = \bar{M}(P - P_z) = \frac{\bar{M}\bar{\gamma}_{sb}}{\bar{R}}\left[\frac{1}{4} - Z\right] \tag{6}$$

with $Z = (\bar{P}_z\bar{R})/\bar{\gamma}_{sb}$ (Humphreys, 1997a). $\bar{M}$ is the mean subgrain mobility and $\bar{R}$ the mean radius of subgrains.

$Z = 0.23$ for *Goss1 h* with $\bar{R} = 2.45\mu m$ and $Z = 0.33$ for *Goss24 h* with $\bar{R} = 2.3\,\mu m$. With these values of Z, the limiting subgrain size by normal growth is comparable with the value of the subgrain size determined after deformation. Therefore, normal subgrain growth could not occur during annealing at 400°C. As a consequence, abnormal subgrain growth is required for nucleation.

From Humphreys (1997a), the growth rate of a particular subgrain of radius R is given by:

$$\frac{dR}{dt} = M(\theta)\left(\frac{\bar{\gamma}_{sb}}{\bar{R}} - \frac{\gamma_{sb}(\theta)}{R} - \frac{Z\gamma_{sb}(\theta)}{\bar{R}}\right) \tag{7}$$

The condition leading to abnormal subgrain growth is $(d(R/\bar{R}))/\,dt > 0$. Abnormal growth occurs when a particular subgrain grows more rapidly than the average grain. The variation of the mobility and the specific energy of boundaries with misorientation (θ) is considered.

The conditions for instability depend on the size, boundary energy and mobility of a grain relative to the grain assembly (Humphreys, 1997b). From Humphreys (1997a), with the values of Z determined above and with a mean misorientation of about 5°, a critical size ratio ($R/\bar{R}$) of about 1.5 appears to be a lower bound for instability. The upper limit for $R/\bar{R}$ is high whatever the value of the boundary misorientation θ.

In conclusion, abnormal growth can give subgrains sufficiently large for nucleation. The only critical conditions are lower bounds for θ and $R/\bar{R}$.

4.3. Nucleation Controlled Textures

We have seen above that recovery by normal growth cannot produce subgrains with a size sufficiently large to induce grain nucleation. Abnormal growth appears to be a necessary and likely nucleation process for the two Goss samples. Due to the effect of both size and misorientation on the subgrain growth rate (Eq. (7)), potential nuclei are not inevitably the biggest before abnormal growth. A subgrain with a relatively small size can grow faster than a large subgrain if its misorientation is higher.

As a consequence, the size advantage of cube subgrains (Ridha and Hutchinson, 1982) cannot be assumed after abnormal subgrain growth. The weak recrystallization texture observed at 400°C seems to indicate that there is no strong correlation between size, misorientation and orientation during abnormal subgrain growth.

Recrystallization textures obtained with the *Goss1 h* sample, but annealed at 510°C, exhibit a significant cube component (Fig. 8). As discussed above, at this temperature, Mg_2Si should be dissolved in the first part of the annealing time and Al-Fe-Si precipitates become rapidly coarser by coalescence. In this case, large cube subgrains can be obtained by normal growth.

Apparently, results obtained in this work contradict previous work on the effect of particles on recrystallization. According to Engler *et al.* (1996) and Benum and Nes (1997), cube oriented subgrains having a size advantage would not be affected by precipitation. However, their samples having been deformed by cold rolling, cube

oriented subgrains are expected to have a size exceeding the critical Gibbs–Thompson diameter for nucleation. Abnormal subgrain growth would not be required for nucleation. As a consequence, the fine precipitation would strengthen the cube component after recrystallization.

5. CONCLUSION

Recrystallization of Al-Mg-Si alloy samples deformed and annealed at 400°C appears to be controlled by fine Al-Fe-Si and Mg_2Si precipitates. Recovery by normal growth does not appear to produce subgrains with a size sufficiently large to induce nucleation. Abnormal subgrain growth is therefore required for nucleation. The weak textures observed after recrystallization indicate that cube subgrains have not the size advantage as found after normal subgrain growth.

A recrystallization texture with a significant cube component was observed after annealing at 510°C on samples presenting a very low fraction of cube volumes before and after deformation. Due to the reduction of the Zener pressure during the first part of the annealing time at 510°C, grain nucleation does not involve abnormal subgrain growth and the observed texture should be the result of the size advantage of subgrains gained during the normal subgrain growth.

Acknowledgments

The material was supplied by the Pechiney research center in Voreppe, France. This research was funded by the Région Rhône–Alpes as part of the AVENIR project. The author would like to thank P. Donnadieu (LTPCM, Grenoble) for her help in the observation of precipitates by TEM.

References

Akef, A. (1993). Déformation en compression plane et recristallisation de monocristaux d'aluminium. *PhD thesis*, Ecole Nationale Supérieure des Mines de Saint Etienne, France.

Beaudoing, A.J., Mecking, H. and Kocks, U.F. (1996). Development of localized orientation gradients in fcc polycrystals. *Phil. Mag.*, **73**, 1503–1517.

Benum, S. and Nes E. (1997). Effect of precipitation on the evolution of cube recrystallization texture. *Acta. Mater.*, **45**, 4593–4602.
Bunge, H.J. (1993). *Texture Analysis in Materials Science*, Cuviller Verlag, Gottingen.
Chan, H.M. and Humphreys, F.J. (1984). Effect of particle stimulated nucleation on orientation of recrystallized grains. *Acta. Metall.*, **32**, 235–243.
Daaland, O. and Nes, E. (1996). Recrystallization texture development in commercial Al-Mn-Mg alloys. *Acta Mater.*, **44**, 1413–1435.
De La Chapelle, S. (2000). Recristallisation d'un alliage Al-Mg-Si; développement des textures et effet de la précipitation. PhD thesis, Ecole Nationale Supérieure des Mines de Saint Etienne, France.
De La Chapelle, S. (2001). Cube recrystallization textures in a hot deformed Al-Mg-Si alloy. *Scripta Materialia*, **45**, 1387–1391.
Engler, O., Yang, P. and Kong, X.W. (1996). On the formation of recrystallization textures in binary Al-1.3% Mn investigated by means of local texture analysis. *Acta Mater.*, **44**, 3349–3369.
Engler, O., Tap, M., Hirsch, J. and Gottstein, G. (1996). Control of the recrystallization textures in Al-Mg-Si sheet alloys. In: Xi'an, Liang, Z., Zuo, L. and Chu, Y. (eds.), *Proc. of Eleventh Int. Conf. on Textures of Materials*. China: Beijing. pp. 405–410.
Ferry, M. and Humphreys, F.J. (1996). Discontinuous subgrain growth in deformed and annealed (110) ⟨001⟩ aluminium single crystals. *Acta Mater.*, **44**, 1293–1308.
Higginson, R.L., Aindow, M. and Bate, P.S. (1997). The effect of finely dispersed particles on primary recrystallization textures in Al-Mn-Si alloys. *Mat. Sci. and Eng.*, A**225**, 9–21.
Hillert, M. (1965). On the theory of normal and abnormal grain growth. *Acta Metall.*, **13**, 227–238.
Huang, Y. and Humphreys F.J. (1999). Measurements of grain boundary mobility during recrystallization of a single-phase aluminium alloy. *Acta Mater.*, **47**, 2259–2268.
Humphreys, F.J. (1977). The nucleation of recrystallization at second phase particles in deformed aluminum. *Acta. Metall.*, **25**, 1323–1344.
Humphreys, F.J. and Hatherly, M. (1995). *Recrystallization and Related Annealing Phenomena*, Pergamon Press, Oxford.
Humphreys, F.J. and Ardakani, M.G. (1996). Grain boundary migration and Zener pinning in particle-containing copper crystals. *Acta. Mater.*, **44**, 2717–2727.
Humphreys, F.J. (1997a). A unified theory of recovery, recrystallization and grain growth, based on the stability and growth of cellular microstructures-II. The effect of second-phase particles. *Acta Mater.*, **45**, 5031–5039.
Humphreys, F.J. (1997b). A unified theory of recovery, recrystallization and grain growth, based on the stability and growth of cellular microstructures-I. The basic model. *Acta Mater.*, **45**, 4231–4240.
Kamijo, T.H., Adachihara, H. and Fukutomi, H. (1993). Formation of a (001)⟨100⟩ deformation structure in aluminum single crystals on an S-orientation. *Acta Metall. Mater.*, **41**, 975–985.
Maurice, C. and Driver, J.H. (1993). High temperature plane strain compression of cube oriented aluminum crystals. *Acta Metall. Mater.*, **41**, 1653–1664.
Murr, L.E. (1975). *Interfacial Phenomena in Metals and Alloys*, Addison-Wesley, Reading.
Nes, E. (1976). The effect of a fine particle dispersion on heterogeneous recrystallization. *Acta Metall.*, **24**, 391–298.
Panchanadeeswaran, S. and Field, D.P. (1995). Texture evolution during plane strain deformation of aluminum. *Acta Metall. Mater.*, **43**, 1683–1692.
Read, W.T. (1953). *Dislocations in Crystals*, MacGraw Hill, New York.

Ridha, A.A. and Hutchinson, W.B. (1982). Recrystallization mechanisms and the origin of cube texture in copper. *Acta Metall.*, **30**, 1929–1939.

Rollett, A.D., Srolovitz, D.J. and Anderson, M.P. (1989). Computer simulation of grain growth-anisotropic grain boundary energies and mobilities. *Acta Metall.*, **37**, 1227–1240.

Smith, C.S. (1948). Grains, phases and interphases: an interpretation of microstructures. *Trans. Metall. Soc. A.I.M.E.*, **175**, 15–51.

Samadjar, I. and Doherty, R.D. (1998). Cube recrystallization texture in warm deformed aluminum: understanding and prediction. *Acta Mater.*, **46**, 3145–3158.

Vatne, H.E., Shahani, R. and Nes, E. (1996). Deformation of cube-oriented grains and formation of recrystallized cube grains in a hot deformed Al-Mg-Mn aluminium alloy. *Acta Mater.*, **44**, 4447–4462.

Zajac, S., Bengtsson, B., Johansson, A. and Gullman, L.O. (1996). Optimisation of Mg_2Si phase for extrudability of AA 6063 and 6005 alloys. *Mat. Sci. Forum*, 217–222, 397–402.